Dynamic Stabilization of the Inverted Pendulum

C. Marcotte,[1] B. Suri,[1] J. J. Aguiliar,[1] and G. Lee[1]
School of Physics, Georgia Institute of Technology, Atlanta, Georgia 30332,
USA

The inverted pendulum is a canonical problem in both Nonlinear Dynamics[1] and Control Theory[2,3]. In this article, the phenomenon of dynamic stabilization of the vertically driven inverted pendulum is investigated experimentally and numerically. We resolve the first stabilizing boundary in driving parameter space, as well as investigate the effects of frictional damping on the dynamics of the pendulum. We finish our investigations with the dynamics of the Double Inverted Pendulum.

I. INTRODUCTION

Originally investigated by P. L. Kapitza[4], and later, Kalmus[5], the inverted pendulum has been shown to have a stable inverted state when it's central pivot is subject to high-frequency vertical displacement under a variety of waveforms.[6] On the subject of dynamical stability, Kapitza had this to say:

> [T]he striking and instructive phenomenon of dynamical stability of the turned pendulum not only entered no contemporary handbook on mechanics but is also nearly unknown to the wide circle of specialists... ...[The phenomenon of dynamical stability is] not less striking than the spinning top and as instructive.[7]

We begin with a short investigation of the theory of dynamic stabilization before continuing to the experimental Methods and Discussions.

II. THEORY

The driven inverted pendulum possesses a rotational symmetry about the vertical axis; to simplify the analysis, we look at solely planar oscillations. Such a system is replicated experimentally. For an inverted pendulum of mass m and length ℓ, affixed at a pivot at position y with angular displacement from the vertical up
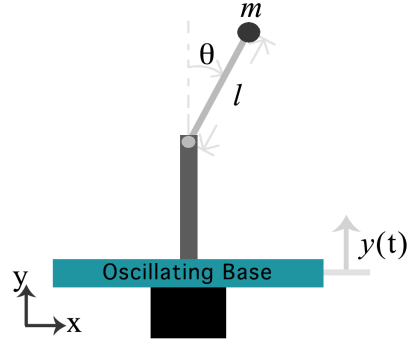

FIG. 1. Diagram of the theoretical model of the inverted pendulum.

position given by θ, the Lagrangian is given by Eq. 1.

$$\mathcal{L} = \tfrac{m}{2}(\ell^2\dot{\theta}^2 + \dot{y}^2 + 2\ell\dot{y}\dot{\theta}\sin\theta) \\ -mg(y + \ell\cos\theta) \qquad (1)$$

Which gives the equation of motion, in scaled, dimensionless parameters $\alpha = g/\ell\omega^2$, $\beta = b/\ell$ and $\tau = \omega t$,

$$0 = \ddot{\theta} + (\beta f(\tau) - \alpha)\sin\theta \qquad (2)$$

Such that $\partial_\tau^2 y(t) = bf(\tau)$, and $\ddot{\theta}$ is understood to be differentiated with respect to τ. We introduce damping to the model through the addition of a frictional term to Eq. 2, where $\hat{\dot{\theta}}$

is the sign of $\dot{\theta}$ and γ is a constant friction coefficient.[8]

$$0 = \ddot{\theta} + \gamma\hat{\dot{\theta}} + (\beta f(\tau) - \alpha)\sin\theta \qquad (3)$$

Clearly, a system described by Eq. 2 possesses two equilibria: $(\theta^*, \dot{\theta}^*)_+ = (0,0)$ corresponding to the upward vertical and $(\theta^*, \dot{\theta}^*)_- = (\pi, 0)$ for the downward vertical. Linearizing around the equilibria and making the perturbative substitution $\eta_\pm = \theta^*_\pm + \delta\theta_\pm$, we obtain the Mathieu equation[9].

$$\delta\ddot{\theta}_\pm \mp (\beta f(\tau) - \alpha)\delta\theta_\pm = 0 \qquad (4)$$

The linear stability analysis confirms our suspicions: the stability of the $(\pm)$-states is determined by the pre-factor $(\alpha - \beta f(\tau))$, with the $(+)$-state losing stability as $\beta \to 0$. It

has been well documented[10] that Eq. 4, governing the stability of the inverted state, implies the existence of a series of bifurcations and "resurrections" as the driving amplitude is varied for fixed driving frequency. With this in mind, limited by the equipment, we resolved only the lower boundary of the first stable region over a range of values for the relevant parameters.

For completeness, we will here include the governing equations for a series-connected double pendulum with the first pivot driven sinusoidally. Solved for using the same Lagrange-Euler formalism as in the single pendulum case, we determine two second-order, nonlinear, coupled differential equations in the variables θ_1 and θ_2, which are the angular displacements of the inner and outer arms of the pendulum, respectively.

$$\ddot{\theta}_1 = -\frac{m_2(L_1\dot{\theta}_1^2\sin(2\theta_1-2\theta_2)+2L_2\dot{\theta}_2^2\sin(\theta_1-\theta_2))+g((2m_1+m_2)\sin(\theta_1)+m_2\sin(\theta_1-2\theta_2))-\ddot{y}((2m_1+m_2)\sin(\theta_1)+m_2\sin(\theta_1-2\theta_2))}{2L_1\big(m_2\sin(\theta_1-\theta_2)^2+m_1\big)}$$

$$\ddot{\theta}_2 = \frac{L_2m_2\dot{\theta}_2^2\sin(2\theta_1-2\theta_2)\ +(m_1+m_2)\big(2L_1\dot{\theta}_1^2\sin(\theta_1-\theta_2)+g(\sin(2\theta_1-\theta_2)-\sin(\theta_2))\big)+\ddot{y}(m_1+m_2)(\sin(\theta_2)-\sin(2\theta_1-\theta_2))}{2L_2\big(m_2\sin(\theta_1-\theta_2)^2+m_1\big)} \qquad (5)$$

III.   METHODS

A.   The Pendulums

There are three iterations of the pendulum represented in this article. The first two are single pendulums, and the third is a series-connected double pendulum.

1.   *The First*

The first pendulum was constructed from aluminum, with an effective length of 6.88 cm. It consisted of a central rectangular rod attached to a near-cube component with two embedded high-end skateboard bearings which rotated about an axle supported on the farthest ends. Unfortunately, one of the bearings exhibited "graininess" and introduced a large θ-dependent frictional term, which was especially
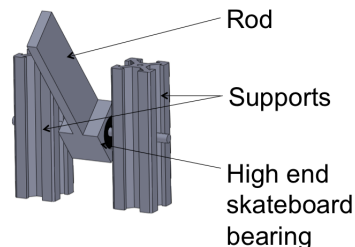

FIG. 2. The first iteration of the pendulum, with effective length 6.88 cm and constructed from aluminum.

pronounced in the vicinity of the fixed point $(+)$ at low angular speeds. This added measurable noise to the measurement of the ring-down, and created small local energy minima causing the pendulum to settle into different angular positions when at rest, which manifested as a "walk-
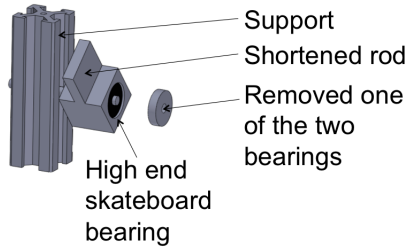
2

FIG. 3. The second iteration of the pendulum, with effective length 3.13 cm and constructed from aluminum. It is **this** iteration which is used for the analysis of the system.
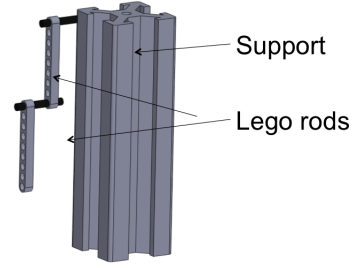

FIG. 4. The final pendulum investigated: the double pendulum. The support is aluminum, and the Lego construction has an effective length of 3.2 cm vertically, while extending approximately 2 cm horizontally from the support.

ing" behavior when driven.

2. The Second

The second pendulum is a modification of the original. Still constructed of aluminum, one of the vertical supports is removed, as well as one of the ball-bearings. Additionally, the arm of the pendulum was drastically shortened. The result is a noticeable improvement in the smoothness of traversal in the vicinity of the fixed point at low angular speeds, and the near elimination of local minima of the energy around the fixed point due to θ-dependent friction. Further, with less mass and a shorter arm, the pendulum is easier to excite, as the amplitude of the driving function is inversely proportional to the pendulum length: $\beta \propto \ell^{-1}$.

3. The Third

The double pendulum was constructed from Lego parts in an asymmetric way such that the pendulums would not collide. This was accomplished by extending each pendulum further from the support than the previous. In this way, the planes described by the "whirling modes" of each separate pendulum do not intersect in space. Unfortunately, due to the flexibility of the axles connecting the pendulums to the sup-

port and each other, when driven the pendulums exhibit large oscillations out of their respective planes. This enables collision of the pendulums, and represents a strongly damped, dissipative mode in addition to the idealized dynamics. The support is the same as before, constructed from aluminum, but the pendulum is affixed by clamps under tension to it.

B. Additional Materials

In addition to the menagerie of pendulums, the use of a shaking table was required, which was outfitted with an accelerometer. The output of the accelerometer was interpreted and displayed on an oscilloscope to measure the peak-to-peak voltage (a measure of the amplitude of the driving function). Further, a function generator and amplifier were used to supply the shaking table with a displacement to attain. For the purposes of tracking the pendulum as the system evolves, electrical tape (in the canonical black), whiteout fluid, and small white plastic spheres were introduced to create regions of arbitrarily high contrast at both the central pivot and the approximate location of the center of mass in the pendulum. Finally, two high-speed cameras were used, one Gray Point for real-time tracking and the other RedLake for offline higher frame-rate tracking, in Labview and MATLAB.

3

C. Collection Methods

To resolve the boundary of the first stability region of the inverted state, in essence, we are spanning a two-dimensional parameter space and measuring the binary value: is the inverted state stable? Practically, we chose a driving frequency on the lower end of the range of available driving frequencies, and with the pendulum slightly displaced from the inverted state, slowly increased the amplitude of the driving waveform until the fixed point becomes locally attractive. For the tracking of the dynamics, high-contrast agents (electrical tape and white-out or white plastic spheres) and two high-speed cameras were used. The real-time tracking algorithm employed in Labview requires several intervening actions from the participants. The first is the manual selection of the tracking markers, followed by setting a threshold to sepa-
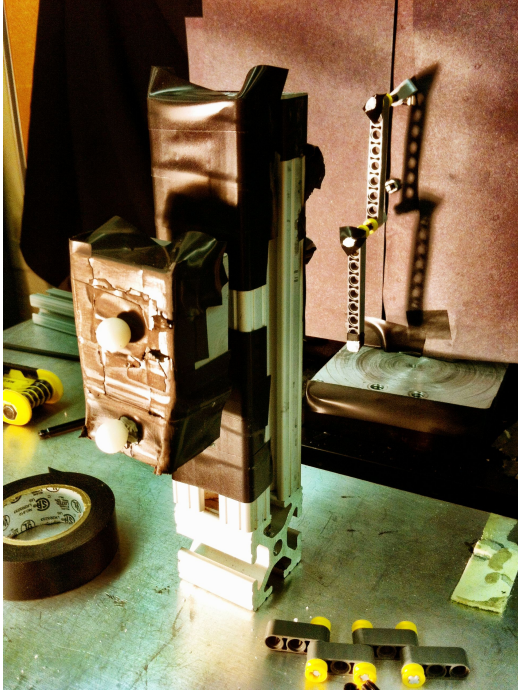

FIG. 5. Photograph of the second and third pendulums, clarifying the use of high contrast markers.

rate the marker highlights from the background. Finally, the program searches a square of points around the initially selected point and finds the center of the pixels which have brightness values above the threshold. This computed center point is then used as the search seed for the next frame, and the process repeats itself. The offline tracking done in MATLAB uses the same algorithm, with a more robust threshold and larger square search size. One issue with this search method is that when obscured, tracking points would become lost or (in the double pendulum case) overlap and merge. To circumvent these issues, and because the algorithm does not interpolate or predict and does not use global information to find the tracking point, we had to manually re-select the tracking points and continue the search.

IV. RESULTS

We begin with the efforts to resolve the stability boundary of the single inverted pendulum state. The results are plotted in Fig. 6. The experimental results are compared to the theoretical predictions in Fig. 7. We include the results of Blackburn, et al, for comparison in Fig. 8.[11]
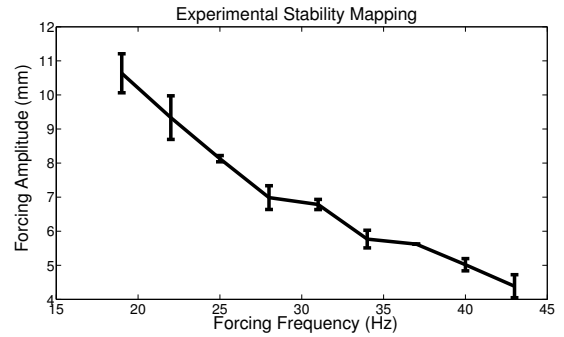

FIG. 6. Experimentally resolved stability boundary of the single inverted pendulum state θ_+.

What follows next is the result of tracking data, and the reconstructed phase portraits thereof. Also included are phase portraits gen-
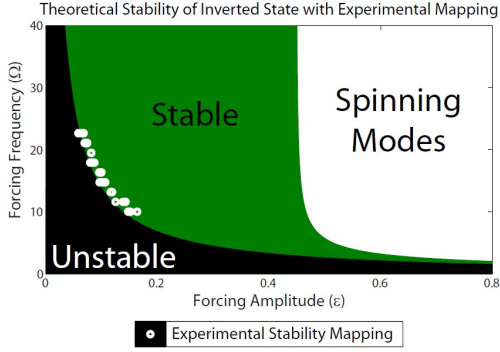
FIG. 7. Experimentally resolved stability boundary of the single inverted pendulum state θ_+. Here, the horizontal axis is scaled such that $\epsilon = \omega_0^2 A/g$, and $\Omega = \omega/\omega_0$, where g is the acceleration due to gravity and $\omega_0 = 2\pi \cdot 1.9\,\text{Hz}$ is the natural frequency of the pendulum, determined from the ring-down tracking data. The experimental data is in white (error bars omitted for clarity), and the theory predicts stability in the green region.
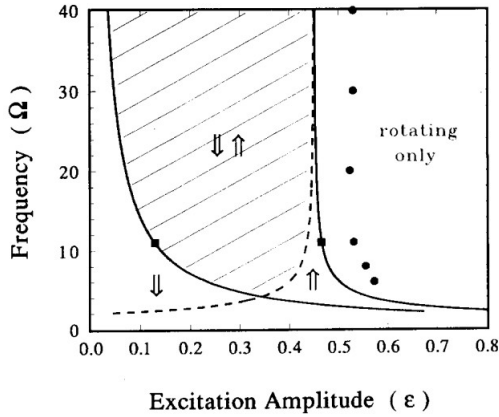

FIG. 8. Results reproduced from Blackburn et al, for the theoretical predictions of the stability boundary.[11]

erated from numerical models of the same system. In short, Fig. 10 should be compared to Fig. 11, and Fig. 12 should be compared to Fig. 13. Note, however, that these phase portraits are, in fact, not phase portraits: the dynamics clearly intersect. These are projections of the space $(\theta, \dot{\theta}, \phi_y)$ onto $(\theta, \dot{\theta})$, where $y(t) = Ae^{i\phi_y t}$.
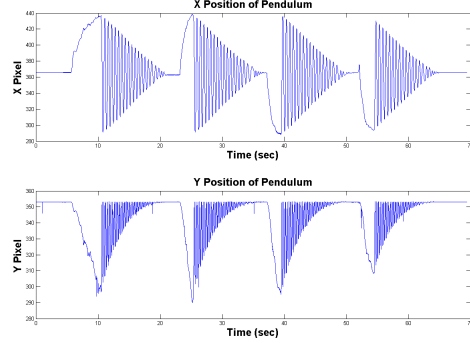

FIG. 9. Raw tracking time-series (x_n, y_n) for the single pendulum, in absolute pixels on the left, with the effect of the driven pivot removed.

To transform the (x_n, y_n, t_n) time-series to a (θ_n, t_n) time-series is simple geometry: $\theta_n = \tan^{-1}(x_n/y_n)$. To construct $\dot{\theta}_n$ is less trivial. Since the temporal spacing is not uniform ($\forall_{i,j\neq i} : t_i - t_{i-1} \neq t_j - t_{j-1}$), spectral methods would require interpolation between the existing data points. This interpolation relies on assumptions about the data set which could introduce systematic errors into the evaluation of $\dot{\theta}$, negating the benefit of computing the derivative spectrally. For this reason, and computational clarity, we chose a nearest-neighbor coupling of the differential operator: $\dot{\theta}_n = (t_n - t_{n-1})^{-1}(\theta_n - \theta_{n-1})$.

Next we present the determination of the damping parameter which corresponds to a constant frictional damping. By fitting a quadratic function to the profile of the θ_n series, we can determine if the damping is frictional (if the profile is linear) or viscous (if the profile is exponential).

Finally, we present the results of our investigations concerning the frequency of small oscillation about the stable inverted state for varied driving frequencies and driving amplitudes.
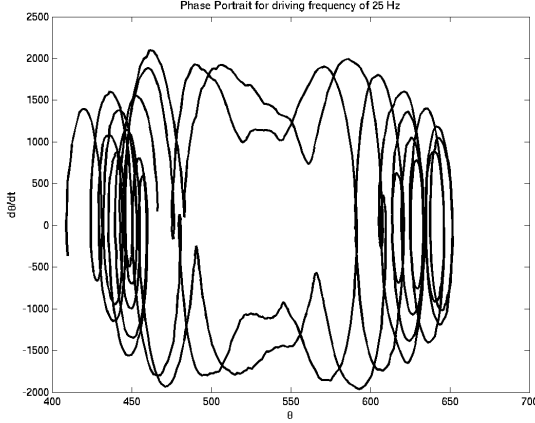
FIG. 10. Phase portrait constructed from the **tracking** of the single pendulum at a driving frequency of 25 Hz. The units on the horizontal and vertical axes are degrees and degrees per second, respectively.
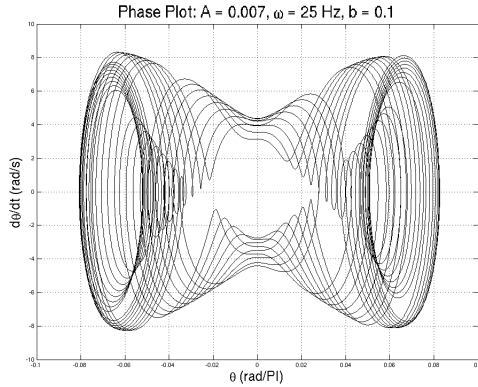

FIG. 11. Phase portrait constructed from simulation of the single pendulum at a driving frequency of 25 Hz. The units on the horizontal and vertical axes are radians/π and radians per second, respectively.

V. DISCUSSION

As concisely put in Fig. 7, over the limited range of driving parameters available to us and the equipment, there is good agreement with
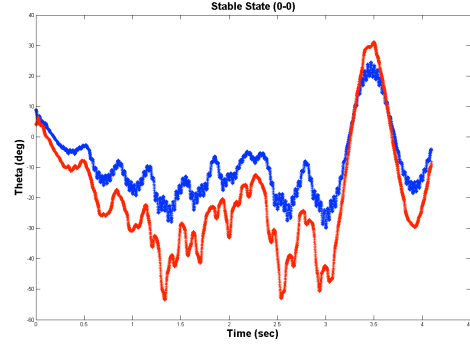

FIG. 12. Time-series representation of $\{\theta_{1,n}, \theta_{2,n}\}$, for the stable-up $(0, 0)$ state under sinusoidal driving of the central pivot, determined **experimentally**.
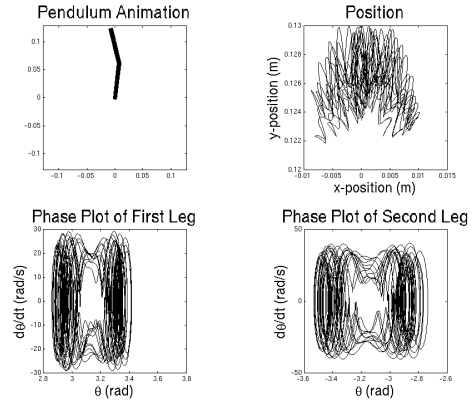

FIG. 13. Verification of the upward-stable state for the series-connected double pendulum under sinusoidal forcing of the central pivot by simulation. In the upper left is a image representation of the $(0, 0)$-state, in the upper right is the extremal position of the outer pendulum arm, and the bottom two plots are phase portraits for the inner pendulum (left) and outer pendulum (right).

theory for the boundary of the first stable region of the inverted state. Further, there is good qualitative agreement in the phase portraits generated from experimental data and numerical simulation, both for the single and dou-
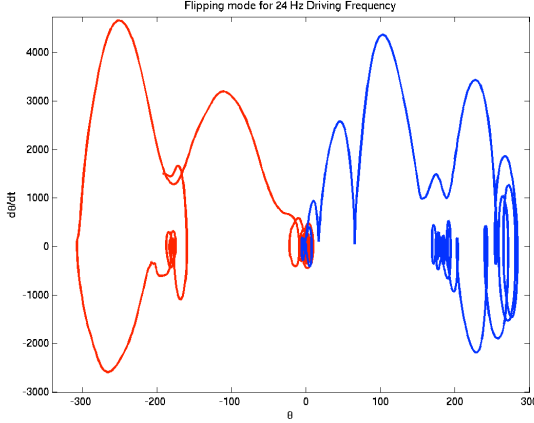
6

FIG. 14. Phase portrait constructed from the **tracking** of the double pendulum at a driving frequency of 24 Hz exhibiting the dynamics of a "flipping" mode. The units on the horizontal and vertical axes are degrees and degrees per second, respectively.
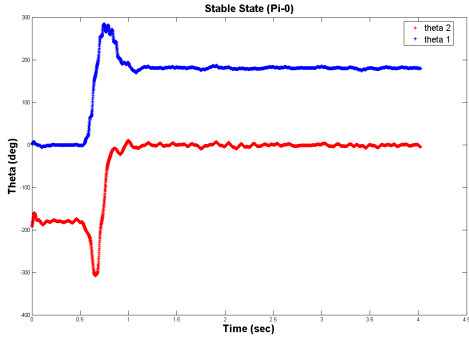

FIG. 15. Time-series representation of the "flipping" mode observed **experimentally** in the double pendulum, included for clarity.

ble pendulums.

Finally, we turn our attention to the "flipping" mode depicted in the phase portrait Fig. 14, and as a time-series in Fig. 15. These are two anti-symmetric states: $(\theta_1, \theta_2) = (0, \pi)$ and $(\pi, 0)$. In this regime, we suspect, the small angle approximation applies to the dynamical
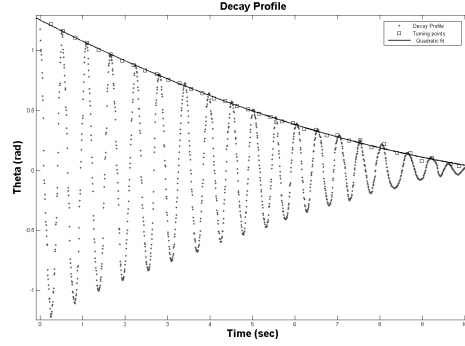

FIG. 16. The results of the "ring down" tracking data, and a quadratic fit to the profile. The fitting-function is a polynomial in t : $f(t; a, b, c) = at^2 + bt + c$. The fit converges with a RMSE of 0.006664, with the pre factor on the quadratic term $\mathcal{O}(b/10)$, indicating a primary contribution to damping which is constant in time, or **frictional**. The pre-factors are $a = 0.0083 \pm 0.000687, 95\%$, $b = -0.198 \pm 0.0054, 95\%$, and $c = 1.28 \pm 0.009, 95\%$.

equations Eq. 5, and small angle deviances of one pendulum may be considered as inertial restoring forces to the other. This explains why the symmetric states $(0, 0)$, (π, π) do not exhibit this phenomenon. As a result, the outer pendulum exhibits nearly independent dynamics. Intuitively, the gauge freedom of the potential energy implies that for these symmetry preserving states the position of the inner pendulum simply defines a higher or lower potential level of the outer pendulum for the $\theta_1 = 0$ and $\theta_1 = \pi$ states, respectively. However, further theoretical work is needed to verify this hypothesis.

VI. CONCLUSION

In conclusion, we were able to stabilize both the single pendulum and the double pendulum using only vertical sinusoidal forcing of the central pivot. We were able to track the dynamics with adequate spatial and excessive temporal resolution and compare their shape to the
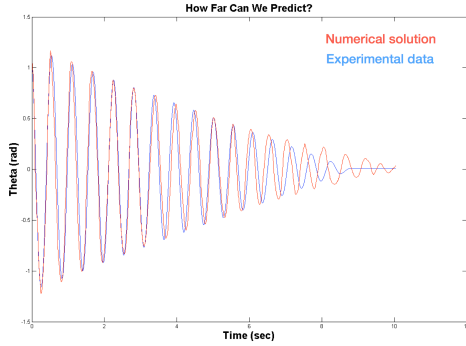
FIG. 17. By fitting over the first oscillatory period with a sine wave and using the previously determined (see Fig. 16) semi-linear profile to determine the form of the damping term in Eq. 3, we may determine the value of the damping coefficient γ. From the fit initial condition and the damping coefficient, the model is integrated in time using an explicit Euler scheme to verify the predictability of the dynamics.
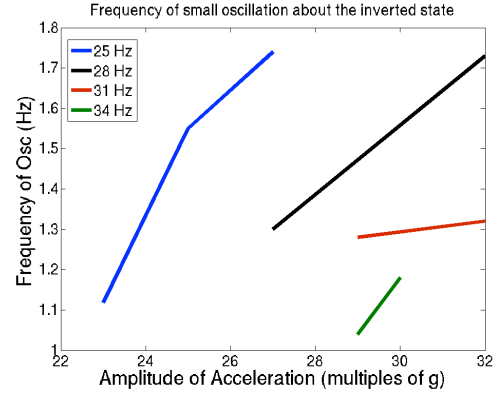

FIG. 18. The results of the investigation into whether the frequency of small oscillations about the inverted state depended on the driving frequency and amplitude. We note a tenuous positive correlation between the amplitude of the acceleration and the frequency of small oscillations about the stable inverted state, $(+)$ for each driving frequency, and across increasing driving frequencies.

simulation results with good qualitative agreement. We resolved the first occurrence of a stability boundary for the single pendulum in the inverted state. Additionally, we were able to observe positive correlation of the frequency of small oscillations about the inverted state for the single pendulum with driving amplitude and frequency. Finally, we observed separable dynamics in a set of antisymmetric states for the double pendulum.

REFERENCES

[1] S. Strogatz, *Nonlinear dynamics and chaos: with applications to physics, biology, chemistry, and engineering* (Perseus Books, 1994).

[2] D. Liberzon, *Switching in Systems and Control* (Springer, 2003).

[3] Franklin, *Feedback control of dynamic systems* (Prentice Hall, 2005).

[4] P. Kapitza, "Dynamical stability of a pendulum when its point of suspension vibrates, and pendulum with a vibrating suspension," Collected Papers of PL Kapitza **2**, 714–737 (1965).

[5] H. Kalmus, "The inverted pendulum," American Journal of Physics **38**, 874 (1970).

[6] E. Yorke, "Square-wave model for a pendulum with oscillating suspension," American Journal of Physics **46**, 285 (1978).

[7] P. L. Kapitza, *Collected papers of P. L. Kapitza*, edited by D. T. Haar, Vol. 2 (Pergamon London, 1976) pp. 714, 726.

[8] A. Marchewka, D. Abbott, and R. Beichner, "Oscillator damped by a constant-magnitude friction force," American journal of physics **72**, 477 (2004).

[9] M. Bartuccelli, G. Gentile, and K. Georgiou, "On the dynamics of a vertically driven damped planar pendulum," Proceedings of the Royal Society of London. Series A: Mathematical, Physical and Engineering Sciences **457**, 3007 (2001).

[10] S. Kim and B. Hu, "Bifurcations and transitions to chaos in an inverted pendulum," Physical Review E **58**, 3028 (1998).

[11] J. Blackburn, H. Smith, and N. Grønbech-Jensen, "Stability and hopf bifurcations in an inverted pendulum," American journal of physics **60**, 903–908 (1992).